Class of cooperative stochastic models: Exact and approximate solutions, simulations, and experiments using ionic self-assembly of nanoparticles

I. Mazilu, D. A. Mazilu, R. E. Melkerson, E. Hall-Mejia, G. J. Beck, and S. Nshimyumukiza
Department of Physics and Engineering, Washington and Lee University, Lexington, Virginia 24450, USA

Carlos M. da Fonseca
Department of Mathematics, Kuwait University, Safat 13060, Kuwait
(Received 24 August 2015; revised manuscript received 1 December 2015; published 25 March 2016)

We present exact and approximate results for a class of cooperative sequential adsorption models using matrix theory, mean-field theory, and computer simulations. We validate our models with two customized experiments using ionically self-assembled nanoparticles on glass slides. We also address the limitations of our models and their range of applicability. The exact results obtained using matrix theory can be applied to a variety of two-state systems with cooperative effects.

DOI: 10.1103/PhysRevE.93.032803

I. INTRODUCTION

Two-state stochastic models with cooperative effects have been successfully used to describe diverse physical systems ranging from surface kinetics [1] to problems in epidemics [2,3] and voting behavior [4]. A particular application for such models, the dynamics of nanoparticle deposition, is currently an active area of research in nanotechnology studies [5,6] that raises interesting questions on the theoretical front.

The class of cooperative sequential adsorption (CSA) models [7], in which adsorption rates depend upon the occupation of neighboring sites, was solved exactly for the one-dimensional case [8], but higher-dimensional models are less understood [9]. Adding evaporation to such models brings additional complications. One of the standard tools used to study these systems, the empty-interval method [10], fails when evaporation is considered.

Our study is motivated by a very specific experimental problem, the ionic self-assembly of nanoparticles, and builds upon previous work [11]. This class of experiments is referred to in the literature as ionic self-assembled monolayers (ISAMs) [12] and has been successfully used in the creation of antireflective coatings [13]. During the manufacturing process, it is highly desirable to know the analytical relationship between the index of refraction and the particle density on the surface. Our goal is to find ways to predict this particle coverage as a function of time by solving relevant cooperative sequential adsorption models. These models are ideally suited for modeling ISAMs since the deposition process of nanoparticles is stochastic and the deposited nanoparticles are electrically charged, as are the substrate deposition sites, suggesting a cooperative sequential adsorption model with attachment rates dependent on nearest-neighbor site occupation. The cooperative effects of the model are due to the interactions between charged particles and are reflected in the attachment rates, that is, a particle will have a lower probability of attachment if particles of the same charge are already attached to the neighboring sites.

Our focus is the class of cooperative sequential adsorption models with limited evaporation defined on a general lattice. We study and compare two types of such models. The first type consists of cooperative sequential adsorption models where the attachment rates are general functions of the total number of particles present in the system. Because of the overall effect of the lattice occupation on the attachment rates, we will call these models total lattice cooperative sequential adsorption (CSATL) models. The second type of CSA models are the ones for which the attachment rates depend on the occupation of the nearest neighbors (CSANN). For both types of models we discuss the case where evaporation of particles is present, but limited. We will use the abbreviation CSAETL (or CSAENN) when evaporation is present.

We present exact analytical results for the probability distribution and particle density of the CSAETL model using matrix theory. We also discuss the limitations of matrix theory in solving these models. Using mean-field theory and Monte Carlo simulations, we find the range of parameters for which the CSAETL model matches well with the CSAENN one. We further discuss the relevance of our analytical results to ISAM experiments. We show a good fit between our CSAETL model and experimental data for the concentration dependence of the particle coverage. On the experimental side, we report data for the time dependence of particle coverage and interpret it in the context of CSAETL models.

The mathematical results and the analysis presented in this paper can be extended to other physical problems for two-state systems, such as generalized biased random walks with variable step lengths, voting problems, or the spread of epidemics. Our model, which includes evaporation (or detachment) of particles, can account for the mechanism of susceptible-infected-susceptible epidemics, for example [14]. If the lattice considered is a Cayley tree, the model can also be related to the attachment and release of drug molecules on synthetic polymers called dendrimers, a mechanism with potential use as a drug delivery mechanism via drug encapsulation [15,16]. Analytical solutions on Cayley trees were found in [17–19].

In the following section of this paper we describe in detail the experimental process of ionic self-assembly of nanoparticles and its connection to cooperative sequential models. In Sec. III we discuss the general two-state model of particle attachment and detachment and outline the general matrix theory methodology. In Sec. IV we present exact results for CSATL with and without evaporation. We discuss the use

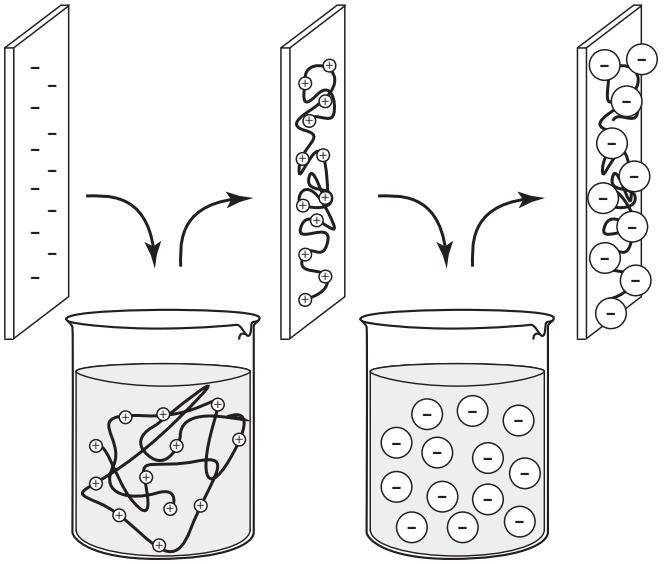

FIG. 1. Sketch of the ISAM process for creating one PDDA-silica bilayer on a glass substrate.

and the limitations of our models in explaining the ISAM experiments in Sec. V. We compare our analytical results to experimental data in Sec. VI and present a summary of our work in Sec. VII.

II. EXPERIMENTAL MOTIVATION: IONIC SELF-ASSEMBLY OF NANOPARTICLES

Ionic self-assembly of monolayers is a quick and low cost process used for the creation of uniform and conformal thin films on charged substrates. The process, sketched in Fig. 1, is based on the sequential layering of oppositely charged ions, typically either alternating charged polyions or using a polyion as an electrostatic glue between layers of ionic nanoparticles [12]. Due to the variety of ions that can be used, the method can yield thin films with vastly different physical structures and allows for the thickness to be controlled with precision on the order of 1 nm [13]. Differing structures, specifically in regard to void space between particles, can alter a film's index of refraction, which is an important factor in the production of optical coatings [20–22]. Our research has focused on alternating layers of cationic polymer, specifically poly(diallyldimethylammonium chloride) (PDDA), with anionic silica nanoparticles. Because of the large nanoparticle size relative to the polymer width, the only observable change during layer-by-layer assembly is due to the silica monolayer of each PDDA-silica bilayer.

We found cooperative sequential adsorption models to be very helpful in modeling the ISAM process. The cooperative aspect of the model captures the electrostatic interactions between the silica nanoparticles. For example, an open site on the lattice that is surrounded by other particles will have a lower probability of attachment compared to open sites with no neighbors. Also included in our model is the stochastic nature of the self-assembly process.

In order to model the ISAM process, we used both CSAETL and CSAENN models. Our CSATL model considers deposition and evaporation rates that are general functions of the overall number of particles present in the system at the time and works for arbitrary size and topology. Natural systems exhibit more subtle behaviors that are often modeled by adsorption and evaporation rates that depend upon the states of cells near a potential adsorption or evaporation site. This dependence on the nearest neighbors is captured by a CSANN model, also presented in [11].

We first discuss the general class of two-state models that lead to useful results for our experiment. We use matrix theory to derive exact solutions for the probability distribution of particle attachment for specific CSA(E)TL models. Unfortunately, this method is limited to only special cases. We further our study by using a mean-field approach to the problem and computer simulation results that show the range of parameters for which our CSATL model can be a good approximation for a CSANN model with nearest-neighbor interactions. In both cases we consider the possibility of particle detachment at a small constant rate.

III. DESCRIPTION OF THE GENERAL TWO-STATE MODEL

Our general model for deposition and evaporation of particles is defined on a grid, in which a set of n connected cells is arranged on a lattice of arbitrary dimension and topology (rectangular grids, Cayley trees, etc.). Our particles are monomers of size equal to the size of a cell on the grid. Each cell of the grid has two states: empty or filled. Empty cells are filled at a rate a_i; filled cells are emptied at a rate b_i. Here a_i and b_i are general functions of the overall number of particles present in the system. This general model can be solved exactly for special cases and it exhibits sufficient complexity to be useful as a standard of comparison for experimental results as well as analytic and computational models that include more complex rate assumptions. Since there is no dependence of the two rates upon the states of any cells other than the cell to be filled or emptied, the results are fully independent of dimension and topology of the grid.

Let P_i represent the time-dependent ensemble-average probability that exactly i cells of the lattice are filled. This obeys the rate equation

$$\frac{dP_i}{dt} = -(a_i + b_i)P_i + a_{i-1}P_{i-1} + b_{i+1}P_{i+1}. \tag{1}$$

This transforms into an equation for the $(n+1)$-dimensional vector P with components $P_0, P_1, \ldots, P_n$ as

$$\frac{dP}{dt} = T_n P,$$

in which T_n is the tridiagonal $(n+1)\times(n+1)$ matrix

$$T_n = \begin{bmatrix} -a_0 & b_1 & & & & \\ a_0 & -(a_1+b_1) & b_2 & & & \\ & a_1 & -(a_2+b_2) & b_3 & & \\ & & a_2 & \ddots & \ddots & \\ & & & \ddots & \ddots & b_n \\ & & & & a_{n-1} & -b_n \end{bmatrix}. \tag{2}$$

For the above matrix, we assume $a_n = 0$, which is justified by the fact that particles will not be able to attach once the lattice is full. In the next section we present general results for the case of nonzero a_n that may be relevant for other physical situations.

In principle, the general time-dependent solution for the elements of vector P is given by

$$P_i = \sum_{k=0}^{n} c_k E_{ik} \exp(\lambda_k t), \tag{3}$$

where λ_k is the kth eigenvalue of T_n and E_{ik} is the ith component of its kth eigenvector. Treating the values E_{ik} as elements of a matrix of eigenvectors, we can use elements of its inverse to solve for the coefficients c_k from a known initial state $P_k(0)$:

$$c_k = \sum_j (E^{-1})_{kj} P_k(0). \tag{4}$$

The knowledge of the probability distribution leads to the possibility to calculate other quantities relevant to experimental work, such as the particle density, for example,

$$\bar{\rho} \equiv \frac{1}{n} \sum_i i P_i, \tag{5}$$

or the standard deviation of the coverage distribution

$$\sigma^2 = \frac{1}{n^2}\left[\sum_i i^2 P_i - \left(\sum_i i P_i\right)^2\right]. \tag{6}$$

However, there are very few tridiagonal matrices with analytical solutions for the eigenvectors and eigenvalues. For example, in a previous work [23] we showed that for the case when the attachment and detachment rates are linear in i, an exact solution is possible for the probability distribution for any initial conditions. In this case, the same results for specific initial conditions can be obtained using the generating function technique. Next we present some useful exact results for special cases of this tridiagonal matrix.

IV. EXACT SOLUTIONS OF SPECIAL CASES USING MATRIX THEORY

A. Cooperative sequential adsorption model

The first case that we discuss is the case of a cooperative sequential adsorption model with no evaporation. Total lattice CSA models a system in which particles attach to the empty sites with general attachment rates a_i. Here a_i can be any general functions of the number of occupied sites i. The results can also be extended for complex functions that may be relevant for other models where oscillatory behavior is present. Detachment of particles is forbidden, therefore $b_i = 0$. In this case, the master equation becomes

$$\frac{dP_i}{dt} = a_{i-1} P_{i-1} - a_i P_i, \tag{7}$$

where i goes from 0 to n (the number of particles in the system), the coefficients a_i are general functions of variable i, and $a_n = 0$. From a physical point of view, $a_n = 0$ means that the lattice is full and the final steady state has a probability $P_n = 1$, while the rest of the probabilities go to zero. Below we present exact results for a more general case that also includes the possibility of a_n being nonzero.

The corresponding transition matrix based on the master equation for P_i is

$$T_n = \begin{bmatrix} -a_0 & 0 & & & & \\ a_0 & \ddots & \ddots & & & \\ & \ddots & -a_{n-2} & 0 & & \\ & & a_{n-2} & -a_{n-1} & 0 & \\ & & & a_{n-1} & -a_n \end{bmatrix}. \tag{8}$$

Because the matrix T_n is triangular, its eigenvalues are the elements of the main diagonal

$$-a_0, -a_1, \ldots, -a_n.$$

An eigenvector associated with the $-a_n$ eigenvalue is clearly

$$(0, \ldots, 0, 1).$$

An eigenvector associated with $-a_i$ is of the form

$$(0, \ldots, 0, \underbrace{*, \ldots, *}_{n-i+1}).$$

The nonzero pattern has the form

$$\begin{aligned} &(-1)^i \prod_{k=i+1}^{n} (a_i - a_k), \\ &(-1)^{i+1} a_i \prod_{k=i+2}^{n} (a_i - a_k), \\ &(-1)^{i+2} a_i a_{i+1} \prod_{k=i+3}^{n} (a_i - a_k), \\ &\vdots \\ &(-1)^n a_i \cdots a_n. \end{aligned}$$

The elements of the inverse of the matrix $A = a_{ij}$ whose columns are the eigenvectors of T_n are

$$a_{ij} = (-1)^{i+j+1}\, a_{j-1} \cdots a_{i-2} \prod_{\substack{k=j-1 \\ k \neq i-1}}^{n} (a_{i-1} - a_k)^{-1}.$$

Notice that the product $a_{j-1} \cdots a_{i-2} = 1$ if $i = j$ and 0 if $i < j$.

B. Cooperative sequential adsorption with limited evaporation

We now include limited evaporation and use matrix theory to explore the possibility of new exact results for the probability distribution. Detachment of particles translates into nonzero b_i's in Eq. (2). We demonstrate the change in the matrix spectrum with the easiest case of a single-particle detachment once the lattice is completely full, with an associated transition

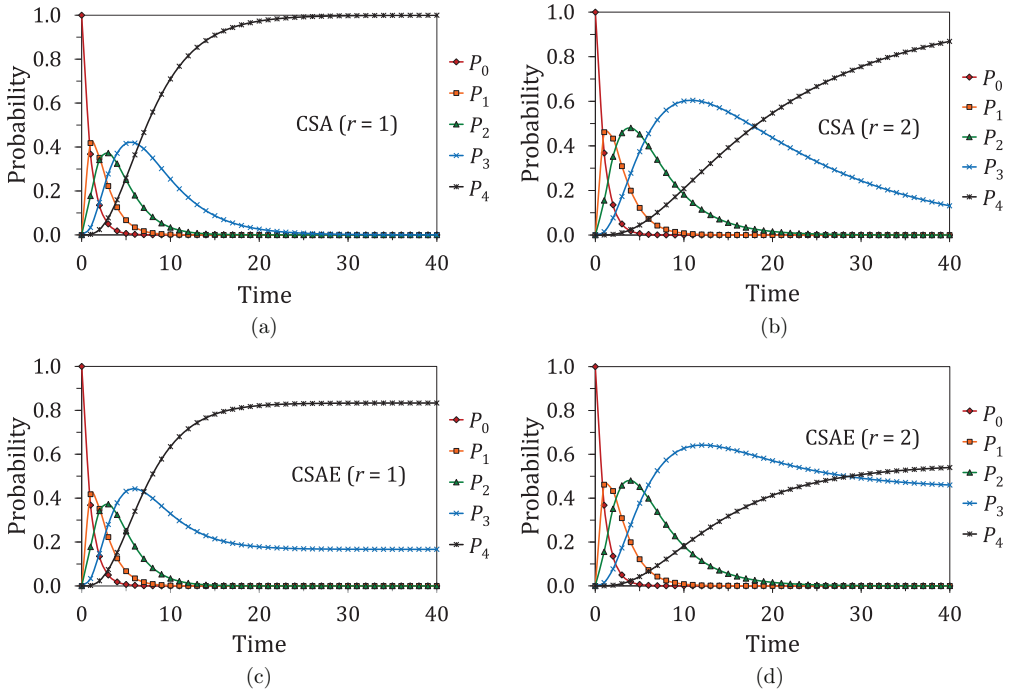

FIG. 2. Probability distribution of an $n = 4$ system as a function of time (in arbitrary units) for (a) attachment rate $a_i = 1 - \frac{i}{n}$ and zero evaporation, (b) attachment rate $a_i = (1 - \frac{i}{n})^2$ and zero evaporation, (c) attachment rate $a_i = 1 - \frac{i}{n}$ and nonzero evaporation, and (d) attachment rate $a_i = (1 - \frac{i}{n})^2$ and nonzero evaporation.

matrix

$$T_n = \begin{bmatrix} -a_0 & 0 & & & \\ a_0 & \ddots & \ddots & & \\ & \ddots & -a_{n-2} & 0 & \\ & & a_{n-2} & -a_{n-1} & b_n \\ & & & a_{n-1} & -b_n \end{bmatrix}. \quad (9)$$

The matrix T_n is not quite triangular and its eigenvalues change slightly. Here a_n is assumed to be zero, which is the relevant case for the particle deposition model. As in the CSATL case, the first $n-2$ eigenvalues are the elements along the main diagonal a_k, with $0 \leqslant k \leqslant n-2$. The eigenvalue $\lambda_k = -a_k - b_n$ corresponds to $k = n-1$ and $\lambda_k = 0$ corresponds to $k = n$.

The eigenvectors change in the following way.

(i) The eigenvector associated with eigenvalue $\lambda_n = 0$ changes its next to last element from 0 to $\frac{b_n}{a_{n-1}}$.

(ii) The eigenvector for eigenvalue λ_{n-1} remains the same.

(iii) In the remaining fractional entries, b_n is subtracted from terms in the numerator that contain a_{n-1}. If a_{n-1} is present only in the denominator (next to the last entry of the remaining eigenvectors), b_n is subtracted from the numerator.

For a more general case of particle detachment, we can find the eigenvalues of the system for the case of a tridiagonal matrix of this type:

$$T_n = \begin{pmatrix} -a_0 & & & & \\ a_0 & -a_1 & b_1 & & \\ & a_1 & -a_2 - b_1 & & \\ & & a_2 & -a_3 & b_2 \\ & & & a_3 & -a_4 - b_2 \\ & & & & a_4 & \ddots \end{pmatrix}.$$

The last block of T_n on the right lower corner is

$$\begin{pmatrix} -a_{n-2} & b_{(n-1)/2} \\ a_{n-2} & -b_{(n-1)/2} \end{pmatrix}.$$

If we view T_n in terms of a block partitioned matrix, the matrix is a block lower triangular matrix. Therefore, the eigenvalues of T_n are in fact the eigenvalues of each main diagonal block. In this case they are

$$0, -a_0, -a_{n-2} - b_{(n-1)/2}$$

and

$$-\tfrac{1}{2}[a_{2i-1} + a_{2i} + b_i \pm \sqrt{-4a_{2i-1}a_{2i} + (a_{2i-1} + a_{2i} + b_i)^2}]$$

for $i = 1, 2, \ldots$. This pattern for the eigenvalues continues no matter the size of the matrix, as long as there is at least one zero on the off-diagonal that contains b's, with the appropriate change in the index for a's.

The eigenvectors for large system sizes become intractable. Numerical results for the eigenvectors and the associated matrix inverse can be found for small finite matrices. It is worth noting that this model can be mapped onto a dual cooperative sequential evaporation with limited evaporation model via a simple translation $a_i \to a_{n-i}$.

Figure 2 shows the significant change in the probability distribution due to a small evaporation rate of $b_n = 0.05$ consistent with Eq. (9). We considered a small system of $n = 4$ particles with attachment rates of the following form: $a_i = (1 - \frac{i}{n})^r$, where $r = 1$ for Figs. 2(a) and 2(c) and $r = 2$ for Figs. 2(b) and 2(d).

As expected, when the evaporation is zero, the steady state is reached when the lattice is full, therefore the probability $P_4 = 1$ for this scenario of $n = 4$. In all cases, P_0 decays

exponentially, with rate a_0. The other probabilities peak at different times, but eventually tend to zero in the steady state. Comparing Fig. 2(a) with Fig. 2(c), we notice that the curves for P_0, P_1, and P_2 have the exact same equations for CSA and CSAE; only the equations for P_3 and P_4 are different due to the possibility of evaporation in CSAE. Here P_3 has a higher, nonzero steady-state value in Fig. 2(c). The same pattern holds for the case of quadratic attachment rates, namely, Figs. 2(b) and 2(d), with different, higher peak times for the P_i, with $i = 1, \ldots, 4$.

V. APPLICATIONS OF THE CSAETL AND CSAENN MODELS TO THE ISAM PROCESS

From a practical point of view, the observable for the ISAM process is the particle density defined as the percentage covered of the substrate surface. It is important to know how this particle density varies with time. In order to get an exact solution for the particle density, we need to solve for the associated probability distribution. Matrix theory leads to exact solutions for special cases, but it breaks down for more complex master equations and other methods are needed, such as mean-field or computer simulations.

A. Example of the CSAETL model solved using matrix theory

We first exemplify how to apply the matrix theory for specific attachment and detachment rates for a CSAETL model with attachment rate defined as linear functions of the overall number i of particles present in the system at time t: $a_i = a(n - i)$ and $b_i = bi$, where a and b are positive constants between 0 and 1. This model has the virtue of simplicity and can be solved exactly, but it exhibits sufficient complexity to be useful as a standard of comparison for experimental results as well as analytic and computational models that include more complex rate assumptions. Since there is no dependence of the two rates upon the states of any cells other than the cell to be filled or emptied, the results are fully independent of dimension and topology of the grid.

Let P_i represent the time-dependent ensemble-average probability that exactly i cells of the lattice are filled. This obeys the rate equation

$$\frac{dP_i}{dt} = -[(n-i)a + ib]P_i + (n-i+1)aP_{i-1} + (i+1)bP_{i+1}. \tag{10}$$

This equation transforms straightforwardly into an equation for the $(n+1)$-dimensional vector P with components $P_0, P_1, \ldots, P_n$ as

$$\frac{dP}{dt} = T_n P,$$

in which T_n is the associated tridiagonal $n \times n$ matrix in this case with the elements

$$T_n = \begin{pmatrix} -na & b & & & & \\ na & -(n-1)a-b & 2b & & & \\ & (n-1)a & -(n-2)a-2b & 3b & & \\ & & (n-2)a & \ddots & \ddots & \\ & & & \ddots & \ddots & nb \\ & & & & a & -nb \end{pmatrix}. \tag{11}$$

The general time-dependent solution for the elements of P is given by

$$P_i = \sum_{k=0}^{n} c_k E_{ik} \exp(\lambda_k t), \tag{12}$$

where λ_k is the kth eigenvalue of T_n and E_{ik} is the ith component of its kth eigenvector. The derivation of these eigenvalues and eigenvectors has been presented in [23]:

$$\lambda_k = -k(a+b)$$

and

$$E_{ik} = \sum_{\ell=i-k}^{n-k} (-1)^{i+k+\ell} \eta^{n-k-\ell} \binom{k}{i-\ell} \binom{n-k}{\ell},$$

with $\eta \equiv b/a$.

Treating the values E_{ik} as elements of a matrix of eigenvectors, we can use elements of its inverse to solve for the coefficients c_k from a known initial state $P_i(0)$:

$$c_k = \sum_j (E^{-1})_{kj} P_k(0). \tag{13}$$

Elements of the inverse matrix are simply related to elements of E itself:

$$(E^{-1})_{ij} = (1+\eta)^{-n} E_{n-i,n-j}.$$

The results above will be used to examine in detail the evolution from each of two specific starting configurations: an initially empty grid and an initially filled grid. These cases are easily established experimentally in physical settings where the current model might apply and yield particularly straightforward analytical expressions for interesting physical properties.

1. Initially empty grid

In this case, the $t = 0$ configuration has no deposited particles and is characterized by $P_0 = 1$ and $P_j = 0$ for $j \neq 0$. From Eq. (13) we determine the constant coefficients

appropriate to this case:

$$c_k = \sum_{j=0}^{n} (E^{-1})_{kj}\delta_{j0} = (1+\eta)^{-n} E_{n-k,n} = (1+\eta)^{-n}(-1)^k \binom{n}{k}. \quad (14)$$

Inserting this result into Eq. (12) produces the following expression for P_i:

$$(1+\eta)^{-n} \sum_{k,\ell=0}^{n} (-1)^{i+\ell} \eta^{n-k-\ell} \binom{n}{k}\binom{k}{i-\ell}\binom{n-k}{\ell} e^{-k(a+b)t},$$

which can be manipulated simply into the form

$$(1+\eta)^{-n} \frac{n!}{(n-i)!} \sum_{\ell} \frac{(-1)^{i+\ell}\eta^{n-\ell}}{(i-\ell)!\ell!} \sum_{k} (\eta z)^{-k} \binom{n-i}{k+\ell-i},$$

where $z \equiv \exp[(a+b)t]$.

The k sum is evaluated as

$$\sum_{k} (\eta z)^{-k} \binom{n-i}{k+\ell-i} = (\eta z)^{\ell-i} \left(1+\frac{1}{\eta z}\right)^{n-i},$$

leaving P_i (after some simplification)

$$(-1)^i \frac{n!}{(n-i)!} \left(\frac{\eta}{1+\eta}\right)^n (\eta z)^{-i} \left(1+\frac{1}{\eta z}\right)^{n-i} \times \frac{1}{i!} \sum_{\ell} (-z)^{\ell} \binom{i}{\ell}.$$

The ℓ sum evaluates to $(1-z)^i$, producing the result

$$P_i = \binom{n}{i} \left(\frac{1+\eta z}{(1+\eta)z}\right)^n \left(\frac{z-1}{1+\eta z}\right)^i, \quad (15)$$

giving a simple form for the time evolution of every term in the distribution of occupation probabilities. The P_i's are easily seen to be elements of a binomial distribution

$$P_p(i|n) = \binom{n}{i} p^i (1-p)^{n-i}$$

that gives the probability of getting exactly i successes out of n trials when the probability of success for each trial is p. The value for p in Eq. (15) is

$$p = \frac{z-1}{z(\eta+1)} = \frac{1-\exp[-(a+b)t]}{1+\eta}.$$

Known properties of the binomial distribution produce an expression for the mean coverage

$$\bar{\rho} \equiv \frac{1}{n}\sum_i i P_i = \frac{1-\exp[-(a+b)t]}{1+\eta},$$

in agreement with the mean-field results for this model. Properties of the binomial distribution also allow simple expressions for all moments of the coverage function. Of particular interest is the variance

$$\sigma^2 = \frac{1}{n^2}\left[\sum_i i^2 P_i - \left(\sum_i i P_i\right)^2\right] = \frac{1}{n}\frac{(1-e^{-(a+b)t})(\eta+e^{-(a+b)t})}{(1+\eta)^2}, \quad (16)$$

which expresses the statistical stability of the system at any time during its evolution.

2. *Initially filled grid*

This case closely parallels the previous one, but with an initial state given by $P_j(0) = \delta_{jn}$, which leads to a different set of coefficients c_k:

$$c_k = \sum_{j=0}^{n} (E^{-1})_{kj}\delta_{jn} = (1+\eta)^{-n} E_{n-k,0} = (1+\eta)^{-n}(\eta)^k \binom{n}{k}. \quad (17)$$

Through manipulations like those above, we derive a form for the time dependence of the elements of P:

$$P_i = \binom{n}{i} \left(\frac{\eta(z-1)}{z(1+\eta)}\right)^n \left(\frac{z+\eta}{\eta(z-1)}\right)^i,$$

leading to a form for the time dependence of the mean coverage for this case as

$$\bar{\rho} = \frac{z+\eta}{z(1+\eta)} = \frac{1+\eta\exp(-(a+b)t)}{1+\eta}$$

and its variance

$$\sigma^2 = \frac{1}{n}\frac{\eta(1-e^{-(a+b)t})(1+\eta e^{-(a+b)t})}{(1+\eta)^2}, \quad (18)$$

both of which approach the same late-time limits as for the initially empty case above.

It is worth noting that Eq. (10) can also be solved using the generating function technique, as this is essentially an example of a biased random walk. We used this specific example due to its relative simplicity, but the methodology can be applied to other attachment and detachment rates.

B. Comparison of CSAETL and CSAENN models using mean-field theory and computer simulations

We explore further the use of cooperative sequential adsorption models for the ionic self-assembly of nanoparticles. Based on the analysis above of a special case of CSAETL, we can see that CSAETL models are in general more amenable to analytical solutions than CSAENN models for which local nearest-neighbor interactions lead to strong particle correlations that make the system unsolvable by mean field of matrix theory methods. We want to identify the range of parameters for which CSAETL and CSAENN models are equivalent.

We choose two cooperative sequential adsorption models, CSAETL and CSAENN on a two-dimensional lattice. We introduce the occupation numbers $n_i = 0$ for an empty site and

$n_i = 1$ for an occupied site, with transition rates as follows:

$$c[n_i \to (1-n_i)] = n_i\gamma + \mu(1-n_i)\left(1 - \frac{\sum_{i=1}^{n} n_i}{n}\right) \quad (19)$$

for the CSAETL model and

$$c[n_i \to (1-n_i)] = n_i\gamma + (1-n_i)\alpha\beta^{\eta} \quad (20)$$

for the CSAENN model.

In Eq. (19), the term $\frac{\sum_{i=1}^{n} n_i}{n}$ represents the overall particle density of the grid and it is subtracted from one so that there is a decreasing likelihood of deposition as the grid fills. For each rate, the system is programmed to change state if a randomly generated decimal is less than or equal to the value of the rate equation at the time. The evaporation of particles happens at a constant rate γ in this model.

The CSAENN transition rate [Eq. (20)] does not consider the overall particle density, but instead takes into account the influence of a particle's nearest neighbors via $\eta = \sum_{j\in \mathrm{NN}} n_j$, which is the sum of the occupied sites that neighbor site i. In this particular case we restrict the values of the parameter β between 0 and 1, to model the electrostatic interaction present for the ionic self-assembly of silica particles. Just as in the previous model, there is a constant evaporation rate given by γ, yet the attachment rate has changed considerably. In both cases, the parameters μ and α ensure particle deposition for the case of either an empty lattice or no neighbors present.

The computer simulations were coded in PYTHON and run on a wide range of two-dimensional grids (10×10, 50×50, 100×100, 300×300, 500×500, 700×700, and 1000×1000). We used a standard Monte Carlo algorithm, where sites were picked at random, occupation of neighboring sites is checked, and the transition rates defined above dictate if the site picked changes state. To ensure that a steady state was reached in a simulation, the number of iterations in each simulation was set at 5×10^7. Random number generation utilized the PYTHON built-in random module, which uses the Mersenne twister, a very reliable generator. The evaporation rate γ was kept constant and low at $\gamma = 0.1$ for both cases. To be consistent with the experiments, the initial configurations were all empty lattices.

We derived equations for the particle density in both cases using the mean-field theory. The CSAENN model was previously discussed in [11]. We now give a very short review of the mean-field results.

Given the transition rate from Eq. (20), the number of particles on the lattice changes according to the following equation:

$$\frac{\partial n_i}{\partial t} = -\gamma n_i + (1-n_i)\alpha\beta^{\eta}. \quad (21)$$

In the mean-field approximation [11], the equation for the rate of change of the particle density is

$$\frac{\partial \rho}{\partial t} = -\gamma\rho + (1-\rho)\alpha\beta^{4\rho}. \quad (22)$$

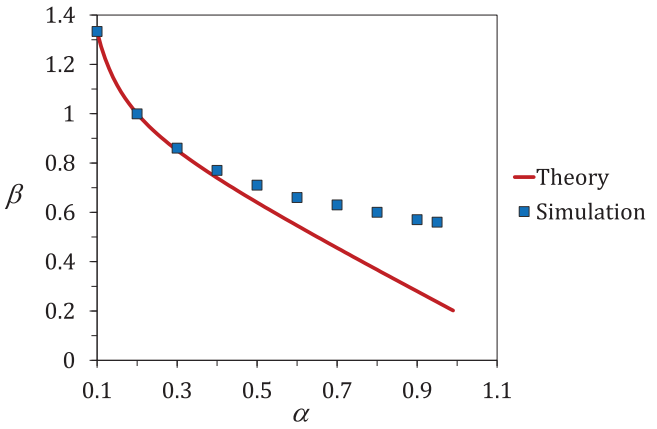

FIG. 3. Comparison of steady states for both models found from mean-field theory (solid line) and simulations (squares). Here $\mu = 0.8$ and $\gamma = 0.1$ for both models.

For the steady state $\frac{\partial \rho}{\partial t} = 0$, this is a self-consistent transcendental equation that can be solved numerically:

$$\rho = \frac{\alpha\beta^{4\rho}}{\gamma + \alpha\beta^{4\rho}}. \quad (23)$$

Although Eq. (23) is a nonlinear function, a linear approximation matches the numerical solution well, as shown in [11]:

$$\rho = \frac{\alpha}{\gamma+\alpha} - (1-\beta)\left[4\left(\frac{\alpha}{\gamma+\alpha}\right)^2\left(1 - \frac{\alpha}{\alpha+\gamma}\right)\right]. \quad (24)$$

Using the same methodology as in [11], we can derive the mean-field equation for the particle density of our CSAETL model as

$$\frac{\partial \rho}{\partial t} = -\gamma\rho + \mu(1-\rho)^2 \quad (25)$$

with an immediate solution for the steady state

$$\rho = \frac{1}{2}\frac{\gamma + 2\,\mu - \sqrt{\gamma^2 + 4\,\gamma\,\mu}}{\mu}. \quad (26)$$

We can match the two steady-state solutions to find the relationship between the parameters for which this match is possible. We also check the validity of this approximation using simulations. Figure 3 shows such a comparison and match for specific values for $\mu = 0.8$ and $\gamma = 0.1$ (the evaporation rate was kept the same for both models). Mean-field theory predicts $\beta = -1.25 \times 10^{-3}(593.1\alpha - 822.1 - \frac{22.2}{\alpha} - \frac{1.4}{\alpha^2})$ for CSAETL and CSAENN to produce matching steady states. As presented in Fig. 3 for a 100×100 lattice, simulations show that the match holds true only for a small range of values, approximately $0.2 \leqslant \alpha \leqslant 0.4$ and corresponding β's. The results for the 100×100 lattice size remains accurate for lattice sizes between 50×50 and 1000×1000, within a margin of error of 3%. A discrepancy appeared for small lattice sizes. For example, for a 10×10 lattice, the first data point in Fig. 3, $(\alpha = 0.1, \beta = 1.38)$, shifts to $(\alpha = 0.1, \beta = 1.42)$ in order for the CSATL and CSANN models to have the same steady states.

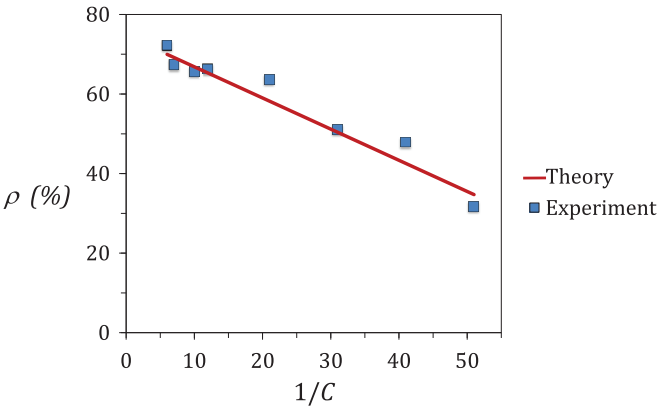

FIG. 4. Comparison of theory and experimental data for the particle density as a function of the inverse of concentration of the colloidal suspension in arbitrary units. The equations associated with the linear fit are from theory (solid line), $y = -0.0077x + 0.7468$ from Eq. (26), and experiment (squares), $y = -0.0078x + 0.7566$ with $R^2 = 0.9468$.

VI. COMPARISON: THEORY AND EXPERIMENTS

We tested the validity of our models in the context of ISAM experiments. In the first set of experiments, presented in the following section, we analyzed how the concentration of the colloidal suspension of nanoparticles affects the steady-state particle density of the thin film. We wanted to see how experimental observables, such as the particle density and suspension concentration, connect to our CSAETL model parameters. In the second set of experiments we analyzed the time dependence of the particle density for a fixed concentration and compared it to the analytical solution provided by the CSAETL model.

A. Concentration dependence

In our experiments we deposited negatively charged spherical silica nanoparticles of nominal 40–50 nm diameter on negatively charged glass slides using poly(diallyldimethylammonium chloride) (PDDA) as polycation, following the steps outlined in Sec. II. The silica nanoparticles (SNOWTEX ST-20L from Nissan Chemical) were in a colloidal suspension at stable pH $= 10.3$ and room temperature $T = 21\,^{\circ}$C. The glass slides were cleaned under sonication, in three successive 20-min steps, with LABTONE detergent, $1N$ sodium hydroxide solution, and deionized water, and then dried with flowing nitrogen gas. The dipping time was 10 min for each bilayer. We varied the concentration of the silica suspension by diluting it with deionized water. We examined the nanoparticle coverage of the substrate using scanning electron microscope (SEM) micrographs, in which deposited particles appear as light regions on a dark background. The details of the experimental procedure to create one-bilayer thin films were also presented in our previous study [11].

We fitted our CSAETL model to the concentration data and found a good match between the two, as shown in Fig. 4. A clear relationship emerges between the parameter μ defined earlier in Eq. (19) and C, the concentration of the colloidal suspension,

$$\mu = e^{-\gamma/2C}. \tag{27}$$

This relationship is valid for low detachment rates $\gamma = 0.1$ and is consistent with the experiments.

The fit with the concentration data works better for low concentrations. At high concentrations, it appears that the evaporation rate is higher and a better fit would be for $\gamma = 0.15$ and $\mu = 0.7$, consistent with the time dependence data presented below.

B. Time dependence

The kinetics of particle adsorption has been studied in [13,20], but there is little consensus in terms of the time scale of the process. In [13] it was reported that silica adsorption onto PDDA reached 90% of its full saturation in 10 s. It seems that for low densities there are two regimes of particle attachment due to the electrostatic screening: a fast Langmuir-type adsorption for a short interval of time followed by a very slow approach to the maximum surface concentration for longer times. The nanoparticles that initially attach to the PDDA glue decrease the probability of attachment for the subsequent nanoparticles from the colloidal suspension. Despite all the time estimates from these studies, there is very little information regarding the kinetics of nanoparticle attachment at times less than 2 s.

An alternative method had to be developed in order to investigate the adsorption of silica nanoparticles at much shorter time scales. We first cleaned the glass slides using a standard method presented in [11]. The clean slides were dipped in a 10 mM PDDA suspension for 10 min and then given three 1-min rinses with deionized water. They were then dried under a nitrogen stream before dipping in the silica nanoparticle suspension.

Each slide was marked beforehand on its side with small, regularly spaced dots and the dipping was done manually. We filmed each dip with a high-speed camera at 1000 frames/s and reviewed the footage measuring how long each dot was in the silica suspension with precision down to the millisecond. This method allowed for each slide to hold many data points, with each dot's horizontal plane being immersed for longer than that above it. We collected a total of 11 data points, ranging from 0.058 s up to 0.639 s.

We examined the nanoparticle coverage of the substrate using SEM micrographs, in which deposited particles appear as light regions on a dark background, and determined the average coverage of light pixels, representing the presence of deposited particles, using a pixel-counting technique. The experimental results are presented in Fig. 5 and compared to the theoretical predictions. The theoretical time was scaled by a factor of 24 to match the real time. The theoretical curve was obtained using the CSAETL model in the mean-field approximation (26) with $\mu = 0.7$ and the evaporation rate $\gamma = 0.2$. We notice that the system settles into a steady state with an overall particle density a little less that 60%, a feature that signifies the presence of evaporation, as well as volume constraints due to particle sizes.

Compared to published studies, it appears that the attachment of particles for one bilayer happens even faster than

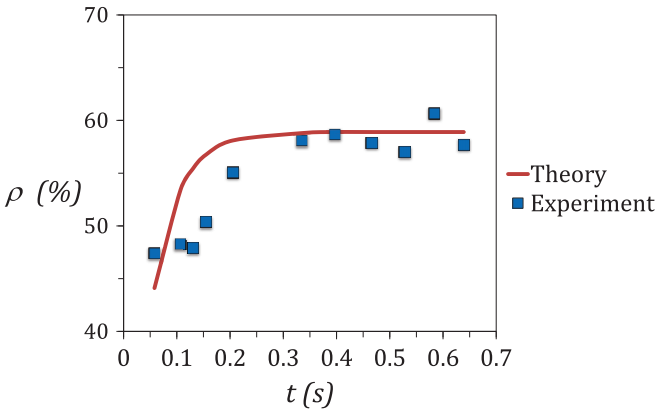

FIG. 5. Time dependence of particle density: experimental data vs theoretical model using the CSAETL model with $\gamma = 0.2$ and $\mu = 0.7$.

previously reported and it exhibits the two regimes mentioned at the beginning of this section. Roughly half of the particles attach in the first 0.058 s, with a slower regime following up to 0.639 s. It was proven in [24] that PDDA in a pure water suspension adsorbs onto a silica surface in a flat rodlike configuration, but adsorbs in random coils in the presence of NaCl. Furthermore, the attractive force between the polyion and colloid is weakened in its presence. The absence of NaCl in our PDDA suspension could have allowed for more uniform adsorption and stronger electrostatic bonding to silica because the charges are not reduced by interaction with counterions. This could provide a possible explanation for the very short time scale of the adsorption process. We find the data intriguing and plan to pursue a more extensive study of the time dependence of the particle coverage.

VII. CONCLUSION

In this paper we discussed in detail a class of cooperative sequential adsorption models relevant to the experimental process of ionic self-assembly of silica nanoparticles. Using matrix theory, we found exact solutions for the probability distribution for general attachment and detachment rates that fit a certain mathematical pattern. We also discussed this model using the mean-field theory and found its limitations in comparison to a previously studied model with nearest-neighbor cooperative effects.

We compared our analytical findings with experimental results for two sets of experiments: concentration dependence of the steady-state particle density and time dependence of the particle density. We found a good fit for our CSAETL model for the concentration dependence data, with a clear relationship between the parameters as reported in Eq. (27). This result leads to the possibility of predicting, for a given concentration of the colloidal suspension, the parameters for the associated analytical model, which, in return, leads to the predicted particle coverage for the steady state. From an experimental standpoint, this method can be both cost and time effective and can be generalized to a concentration-dependent study of the index of refraction of multilayered thin films.

We explored both analytically and experimentally the time-dependent process of particle attachment and detachment. Our preliminary experimental curve (Fig. 5) seems to indicate a much faster time scale of particle attachment than previously reported. It will be interesting to analyze this further for other concentrations and for an even smaller time interval to see if this pattern still holds. Our theoretical curve based on the mean-field approximation of the CSAETL model is a good approximation of the experimental curve but does not capture the two-stage process of particle attachment that the data show.

We hope that the analytical results reported in this paper will be used to understand other two-state systems where cooperative effects are present. Also, the exact results provided by the matrix theory can contribute to finding general matrix spectra for special tridiagonal matrices.

ACKNOWLEDGMENTS

The authors thank David Pfaff for invaluable technical help and Tom Williams and Eric Schwen for helpful conversations. Funding for this research was provided through the Summer Research Scholars Program and the Lenfest Grant at Washington and Lee University.

[1] T. M. Liggett, *Stochastic Interacting Systems: Contact, Voter, and Exclusion Processes* (Springer, Berlin, 1999).
[2] O. Diekmann and J. A. P. Heesterbeek, *Mathematical Epidemiology of Infectious Diseases: Model Building, Analysis and Interpretation* (Wiley, Chichester, 2000).
[3] J. D. Murray, *Mathematical Biology I: An Introduction* (Springer, Berlin, 2002).
[4] C. Castellano, C. Fortunato, and V. Loreto, Rev. Mod. Phys. **81**, 591 (2009).
[5] *Multilayer Thin Films: Sequential Assembly of Nanocomposite Materials*, edited by G. Decher and J. B. Schlenoff (Wiley-VCH, Weinheim, 2003).
[6] M. Di Ventra, S. Evoy, and J. R. Heflin, *Introduction to Nanoscience and Technology* (Springer, New York, 2004).
[7] V. Privman, *Nonequilibrium Statistical Mechanics in One Dimension* (Cambridge University Press, Cambridge, 1997).
[8] M. D. Grynberg, T. J. Newman, and R. B. Stinchcombe, Phys. Rev. E **50**, 957 (1994).
[9] P. L. Krapivsky, S. Redner, and E. V. Ben-Naim, *A Kinetic View of Statistical Physics* (Cambridge University Press, Cambridge, 2010).
[10] D. ben-Avraham and M. L. Glasser, J. Phys.: Condens. Matter **19**, 065107 (2007).
[11] L. J. Cook, D. A. Mazilu, I. Mazilu, B. M. Simpson, E. M. Schwen, V. O. Kim, and A. M. Seredinski, Phys. Rev. E **89**, 062411 (2014).
[12] R. K. Iler, J. Colloid Interface Sci. **21**, 569 (1966).
[13] Y. M. Lvov, K. Ariga, M. Onda, I. Ichinose, and T. Kunitache, Langmuir **13**, 6195 (1997).

[14] T. Tome and M. J. Oliveira, J. Phys. A: Math. Theor. **44**, 095005 (2011).
[15] S. Hecht and J. M. J. Frechet, Angew. Chem. Int. Ed. **40**, 74 (2001).
[16] P. Kolhe, E. Misra, R. M. Kannan, S. Kannan, and M. Lieh-Lai, Int. J. Pharm. **259**, 143 (2003).
[17] A. Cadilhe, N. A. M. Araujo, and V. Privman, J. Phys.: Condens. Matter **19**, 065124 (2007).
[18] A. Cadilhe and V. Privman, Mod. Phys. Lett. B **18**, 207 (2004).
[19] D. A. Mazilu, I. Mazilu, A. M. Seredinski, V. O. Kim, B. M. Simpson, and W. E. Banks, J. Stat. Mech. (2012) P09002.
[20] S. E. Yancey, W. Zhong, J. R. Heflin, and A. L. Ritter, J. Appl. Phys. **99**, 034313 (2006).
[21] M. Ibn-Elhaj and M. Schadt, Nature (London) **410**, 796 (2001).
[22] J. Q. Xi, M. F. Schubert, J. K. Kim, E. F. Schubert, M. Chen, S. Y. Lin, W. Liu, and J. A. Smart, Nat. Photon. **1**, 176 (2007).
[23] C. M. da Fonseca, D. A. Mazilu, I. Mazilu, and H. T. Williams, Appl. Math. Lett. **26**, 1206 (2013).
[24] E. Kokufuta and K. Takahashi, Macromolecules **19**, 351 (1986).